

Texture Evolution in Continuous Casting AA5052 Aluminum Alloy Hot Band During Equi-biaxial Stretching

X. Y. Wen^a, Z. D. Long^a, W. M. Yin^b, T. Zhai^c, Z. Li^d and S. K. Das^b

^a Center for Aluminum Technology, University of Kentucky,
1505 Bull Lea Rd. Lexington KY 40511 USA

^b Secat, Inc.,
1505 Bull Lea Rd. Lexington KY 40511 USA

^c Department of Chemical and Materials Engineering, University of Kentucky,
177 Anderson Hall, Lexington KY 40506

^d Aleris International, Inc.,
1505 Bull Lea Rd., Lexington KY 40511 USA

Abstract In this study, the global texture evolution in a 2 mm gauge hot band of continuous casting AA5052 aluminum alloy, annealed at 449 °C for 4 hours, was investigated. Samples were deformed to three different strain values under a near equi-biaxial stretching condition. Their textures were. The major and minor strains of these samples were measured using an automatic strain analysis system. The texture evolution in the different layers through thickness of these samples was measured using X-ray diffraction. It was found that cube and Goss ($\{110\}\langle 001\rangle$) components varied markedly during biaxial stretching, while brass, copper and S components were changed only slightly. Cube orientation was decreased, whereas Goss orientation was increased, which was more profound in the surface region of the hot band during stretching. A weak fiber-like component, $\{110\}\langle hkl\rangle$, was developed during biaxial stretching. In addition, a $\{110\}\langle 111\rangle$ component was also found to exist mainly in the surface.

Key words: AA5052 Aluminum Alloy, Texture, Continuous casting, Equi-biaxial stretching

1. Introduction

Biaxial stretching is the major deformation form in a stamping operation which is a dominant forming practice in automotive industry. Experimental studies of the deformation behavior of sheet metal during biaxial stretching have been carried out in a wide range of alloys [1-4]. There are few reports, however, available in literature on the effect of grain orientations on the biaxial stretching behavior of sheet metal. The texture development during biaxial stretching of sheet metals was only studied by use of recalculated pole figures with a $\langle 110\rangle$ //ND fiber texture [5].

Crystal orientation is one of the key crystallographic characteristics that determine micro plastic deformation in metals. A model of polycrystal plasticity has been formulated, based on the crystallographic nature of plastic deformation [6]. The origin of rolling texture in face centered cubic metal can be explained using this model [7]. In order to understand orientation change during plastic deformation, several theoretical models have been proposed. However, few of them deals with the texture evolution during biaxial plastic deformation [8, 9].

In the aluminum sheet that is deformed under an approximate plane strain condition (such as rolling), a copper-type rolling texture is formed, which is characterized by the development of preferred orientations along the so-called β -fiber orientation [10]. It has been found that the evolution of the through-thickness texture gradient under rolling conditions can be characterized by the ratio of contact length between roll and sample to sheet thickness [11-13]. Non-uniform deformation mainly due to large friction between rolls and sheet could lead to formation of pronounced shear textures in the surface layers of a rolled sheet [14-16]. However, the texture evolution in aluminum alloy sheet during biaxial deformation has an important effect on the deformation behavior of the sheet, therefore it needs to be investigated.

In this work, the texture evolution through thickness during near equi-biaxial stretching was studied in hot band of the continuous cast AA5052 aluminum alloy annealed at 449°C for 4 hours. Cube and Goss texture components were found to vary significantly during biaxial stretching, unlike in rolling β -fiber component is the main texture to vary.

2. Materials and Experiments

2.1 Materials

The materials used in this work was commercial AA5052 Al alloy hot band produced by the continuous cast (CC) technology. The chemical composition of the alloy is listed in Table 1. The gauge of the hot band was 2.0mm thickness. The hot band was annealed at 449°C for 4hours to obtain an O-temper condition.

Table 1 Composition of experimental materials (wt.%)

Alloy	Si	Fe	Cu	Mn	Mg	Zn	Cr	Al
AA5052 alloy	0.20	0.40	0.05	0.06	2.30	0.06	0.20	Balance

2.2 Plastic deformation and strain analysis

Surface grids were made using electro-chemical etching in samples before biaxial stretch experiments in which a sheet sample was formed into a hemispherical dome by utilizing a Tinius Olsen BUP Ductometer. The hemispherical dome cups were made by a steel sphere of 60 mm in diameter. The bulging deformation was continued until the onset of necking. In these tests, clamping force was about 900kg in order to hold sheet. Finally, the top part of the dome, with about 20 mm x 20 mm area, was cut for strain analysis. Two photographs of the area of interest were taken from different view angles. Computer software used to calculate the 3D shape of the deformed part and the strain distribution across the measured area. After deformation, for each sample, the major and minor strains were measured using the Cam Sys Inc software ASAME Lite (Automated Strain Analysis & Measurement Environment) version 4.1. The procedure followed the ASTM standard E2218-02. Samples were deformed up to three different major strains, 7.87%, 16.3% and 23.3%, respectively, in order to study the texture evolution during biaxial stretching.

2.3 Global texture measurement

A Rigaku D/Max Diffractometer with a multi function stage was used to conduct the pole figure measurement and analysis. Four $\{111\}$, $\{200\}$, $\{220\}$ and $\{311\}$ poles figures for each sample were measured. The alpha rotation angle was from 15° to 90° , and the alpha step was 5° . The four pole figures of $\{111\}$, $\{200\}$, $\{220\}$ and $\{311\}$ were used to conduct Orientation Distribution Functions (ODF) calculation and the volume fractions of texture components, Cube- $\{001\}\langle 100\rangle$; Goss- $\{011\}\langle 100\rangle$; Brass- $\{011\}\langle 211\rangle$; S- $\{123\}\langle 634\rangle$ and Copper- $\{112\}\langle 111\rangle$, were quantified using the Tex Tools software developed by ResMat Corporation. The calculation was based on the series expansion method. The tolerance angle used in the calculation was 15° which is widely used in texture quantification. For the samples deformed at different strain levels and before deformation, the texture evolution was evaluated through thickness, as $S = h/h_0$, where h was the location of the measurement, h_0 the half thickness. If $S = 0$, it was the center of the hot band, and $S = 1$, the surface of the hot band.

2. Results

Microstructure of the O-temper AA5052 hot band appeared to be non-uniform through thickness. As shown in Fig. 1, the grain structure in the surface region was finer than that in the middle where grains were coarse and elongated in the rolling direction. Particles were often observed along grain boundaries, as well as inside grains.

The result of strain analysis is shown in Fig. 2. With increasing in deformation, the size of grids was increased on the surface of the samples. Samples were deformed at major strains of 7.87%, 16.3% and 23.3% respectively. Their Orientation Distribution Functions ($\varphi_2 = 0^\circ, 45^\circ$), together with that of the O-temper hot band, were calculated from pole figure measurement, and are shown in Fig. 3. In Fig. 3, S is a ratio of location/thickness. $S = 1.00$ means the surface layer and $S = 0.50$ means center layer of the hot band. The positions of six ideal orientations in Euler space are illustrated in Fig. 4.

The texture profiles through thickness of all the measured samples are shown in Fig. 5. In addition to the difference in grain structure between the surface and center, the textures in the surface were also different from those in the center in these samples, as shown in Fig. 5. Immediately inside the samples, texture became relatively uniform. Generally, more Goss and $\{011\}\langle 111\rangle$ components and less cube appeared in the surface than in inside the sheet. The rest of the texture components did not show significant variation through thickness before and after biaxial stretching. Before the bulging deformation, cube component was the dominant texture in the O-temper hot band (Fig.5). It was found that the maximum value of the cube component was at $S = 0.7$ location/thickness. The $\{011\}\langle 111\rangle$ orientation was only formed in the surface layer after hot rolling and annealing. The intensity of this orientation on the surface was 3.40 and dropped quickly bellow $S = 0.99$ in the O-temper hot band, but got intensified after stretching.

With increase in major strain during equi-biaxial stretching, several texture components in the surface layer varied. First, cube component was quickly decreased, with increase in strain. The cube component might have been rotated to the Goss orientation, as the Goss component was increased in the surface in this process. From the result of texture measurement (see Figs. 5-8), it can be seen that Goss component was increased slowly in volume fraction inside the sheet, after initial quick increase with strain during biaxial stretching. It might be also possible that part of

Goss component was changed to the Brass orientation, since brass component was increased slightly during the stretching. The $\{011\}\langle 111\rangle$ component was also increased slightly with strain (its intensity increased from 3.4 in the surface at 0% strain to 4.89 at the major strain of 23.3%, which might be due to part of Brass component being rotated to this orientation during the stretching.

It might also be possible that part of r-Goss- $\{110\}\langle 110\rangle$ component was rotated to $\{110\}\langle 111\rangle$ during the biaxial stretching (Fig. 2). This contributed partially to the increase in $\{110\}\langle 111\rangle$ component during equi-biaxial stretching.

4. Discussion

4.1 Rotation of cube

The lattice rotation of polycrystals in rolling and channel die compression has been investigated experimentally and theoretically. Cube component is one of the important recrystallization textures. This orientation is often found to change into two possible orientations during large deformation [17,18]. During hot and cold rolling deformation, one possible path is to r-cube- $\{100\}\langle 011\rangle$ orientation, in which the $\langle 100\rangle$ orientation of cube grains is rotated to $\langle 110\rangle$ orientation as the rolling direction. Another possible path is to Goss- $\{110\}\langle 001\rangle$ orientation, in which $\{001\}$ plane of the cube grains is rotated to $\{011\}$ plane as the rolling plane. In addition, the cube orientation sometimes can also be rotated directly to copper orientation. The first possible path usually occurs, when the strain rate and strain are small. The second takes place often in cold rolling with large reduction and high strain rate for each pass. The last possible rotation path is found to occur in cold rolling where roll reduction is larger than 70% in AA5052 alloys [19]. The grains with cube orientation often have large angle grain boundaries with their neighboring grains in continuous cast Al alloys. In the present work, it was found that the cube component was mainly transformed to Goss orientation during equi-biaxial stretching. The cube grains were easily deformed because of their higher values of Schmid factors, and, therefore, they are rotated quickly during the equi-biaxial stretching.

4.2 Rotation of Goss and R-Goss $\{110\}\langle 110\rangle$

After large reduction in rolling, it has been found that Goss orientation can be completely rotated into brass orientation [20]. With increasing in major strain in biaxial stretching, Goss component can also be rotated to brass orientation. This was the sole path for Goss orientation during deformation. It is the nature of Goss grains that some of them are stable and the others moves to brass orientation in CC aluminum alloys. It was not clear, however, about which grains were stable and which were rotated to Brass orientation during the equi-biaxial stretching. This is in sharp contrast to that strong β fiber texture appears and Goss orientation disappears in heavy rolling deformation.

r-Goss component often caused by shear deformation. It was found that the character of R-Goss component is from R-Goss orientation to $\{110\}\langle 111\rangle$ in copper single crystals in channel die [21]. In this work, on the surface, the rotation can be seen in Fig. 3 ($S=1.0$ and 0.99). In the center layer, the R-Goss component does not almost develop to $\{110\}\langle 111\rangle$ orientation.

4.3 Rotation of Brass- $\{101\}\langle 121 \rangle$

Brass- $\{101\}\langle 121 \rangle$ component is one of the important deformation texture components. It is a relatively stable orientation during rolling and in channel die deformation. It forms the important part of β -fiber texture which is developed in cold rolling. The β -fiber texture runs from brass orientation through S- $\{123\}\langle 642 \rangle$ to copper orientation. There are two active slip systems in a brass grain in an aluminum alloy in channel die deformation [22]. The present work indicated that brass orientation remained almost a constant volume fraction and also might have partially been changed to $\{101\}\langle 111 \rangle$ orientation during equi-biaxial stretching deformation, especially in the surface. The reason might be that the difference between the major and minor stresses in the near equi-biaxial stretching could result in rotation of brass grains to $\langle 111 \rangle$ orientation as the rolling direction. This may indicate that brass orientation can become unstable in a complex stress state.

4.4 Lattice rotation from cube or R-Goss- $\{101\}\langle 101 \rangle$ to $\{101\}\langle 111 \rangle$ orientation

The development of crystallographic orientations during large cold rolling reduction normally leads to formation of a strong β -fiber texture. In a hydraulic bulging test, a $\langle 111 \rangle //$ ND fiber deformation texture appears in an aluminum alloy which has a crystallization texture before deformation [5]. In the present study, it was found that Goss and $\{101\}\langle 111 \rangle$ orientations were stable in the surface during biaxial stretching. Below the surface, brass component was increased only slightly, while cube and Goss components became the main textures that varied with the major strain of biaxial stretching in Al alloy sheet, unlike in rolling and channel die deformation where friction between sample and rollers/die influences the development of texture component. The other factor, a large angle or small angle boundary, also could have a different effect on texture development. This needs further studies by electron back scatter diffraction. In this work, cube component was first changed to Goss orientation, then some of the Goss grains were rotated to brass orientation, and finally to $\{101\}\langle 111 \rangle$ position in the surface. Inside the sheet, Goss and brass orientations were saturated and became stable quickly, while the sheet was being stretched continuously.

5. Conclusions

The deformation behavior during the equi-biaxial stretching was studied. Based on the results obtained, the following conclusions can be drawn:

- 1) The equi-biaxial stretching decreased cube texture quickly;
- 2) In the surface, the $\{101\}\langle 111 \rangle$ texture was formed in the hot band after annealing at 449°C for 4 hours and after stretching respectively;
- 3) In the surface, one possible rotation path for cube component was through Goss and Brass to $\{101\}\langle 111 \rangle$ orientation. Another possible path was through r-Goss to $\{101\}\langle 111 \rangle$.
- 4) Copper- $\{112\}\langle 111 \rangle$ and S- $\{123\}\langle 634 \rangle$ orientations did not vary during equi-biaxial stretching.

6. References

- [1] M. Arin and A. Backofen, Met. Trans. 1, 2857(1970).

- [2] A. K. Tadros and P. B. Metallor, *Int. J. Mech. Sci.* 20, 121(1977).
- [3] R. C. Dorward, *J. Mater. Eng. Perform.* 3, 115(1994).
- [4] X. Y. Wen and W. B. Lee, *Scripta mater.* 43, 1(2000).
- [5] L. S. Toth, J. Hirsch and P. Van Houtte, *Int. J. Mech. Sci.*, 38, 1117-1126(1996)
- [6] G. I. Taylor, *J. Inst. Metals.* 62, 307(1938).
- [7] M. R. Pickus and C. H. Mathews, *J. Inst. Metals.* 64, 237(1939).
- [8] Y. Zhou and K. W. Neale, *Mater. Sci. Forum.* 157-162, 873(1994).
- [9] Y. Zhou, K. W. Neale and L. S. Toth, *Textures and Microstructures.* 14-18, 1055(1996).
- [10] J. Hirsch and K. Lucke, *Acta Metall.* 36, 2863-2882(1988).
- [11] H. O. Asbeck and H. Mecking, *Mater. Sci. Eng.* 34, 111-119(1978).
- [12] W. truskowski, J. Krol and B. Major, *Metall. Trans.* 11A, 749-758(1980).
- [13] O. V. Mishin, B. Bay and D. Juul Jensen, *Metall. Mater. Trans.* 31A, 1653-1662(2000).
- [14] K. K. Mathur, and P. R. Dawson, *Int. J. Plast.* 5, 67-94(1989).
- [15] C. H. Choi, J. W. Kwon, K. H. Oh and D. N. Lee, *Acta Mater.* 45, 5119-5128(1997).
- [16] O. Engler, M. Y. Huh and C. N. Tome, *Metall. Mater. Trans.* 31A, 2299-2315(2000).
- [17] J. Hirsch and K. Lucke, *Acta Metall.* 36, 2883-2904(1988).
- [18] J. Liu and J. G. Morris, *Mater. Sci. Eng.* A357, 277-296(2003).
- [19] J. Liu and J. G. Morris, *Metall. Mater. Trans.*, 34A, 951-966(2003).
- [20] M. Y. Huh, S. Y. Cho and O. Engler, *Mater. Sci. Eng.* A315, 35-46(2001).
- [21] M. Wrobel, S. Dymek and M. Blicharski, *Scripta Mater.* 35, 417-422(1996).

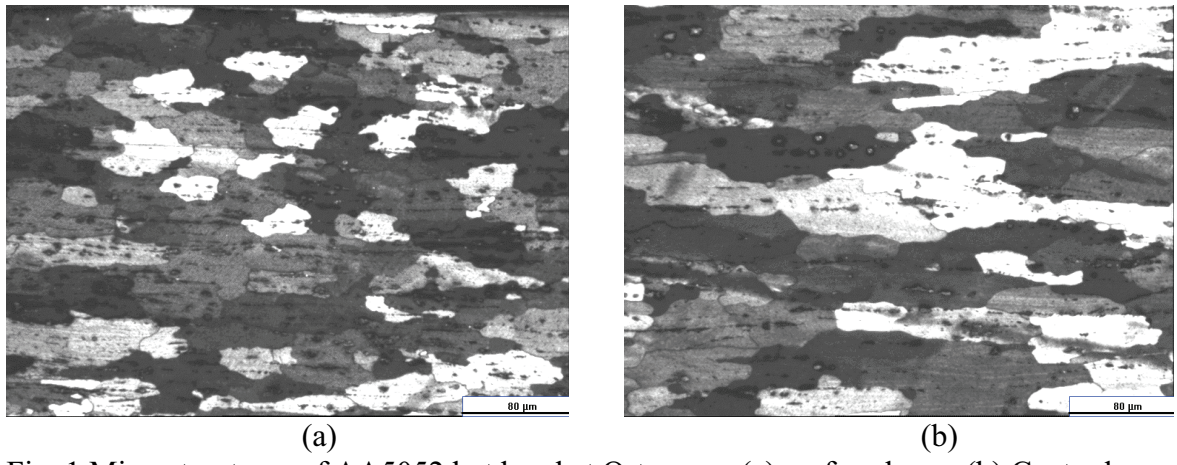


Fig. 1 Microstructures of AA5052 hot band at O-temper, (a) surface layer; (b) Center layer, 200x

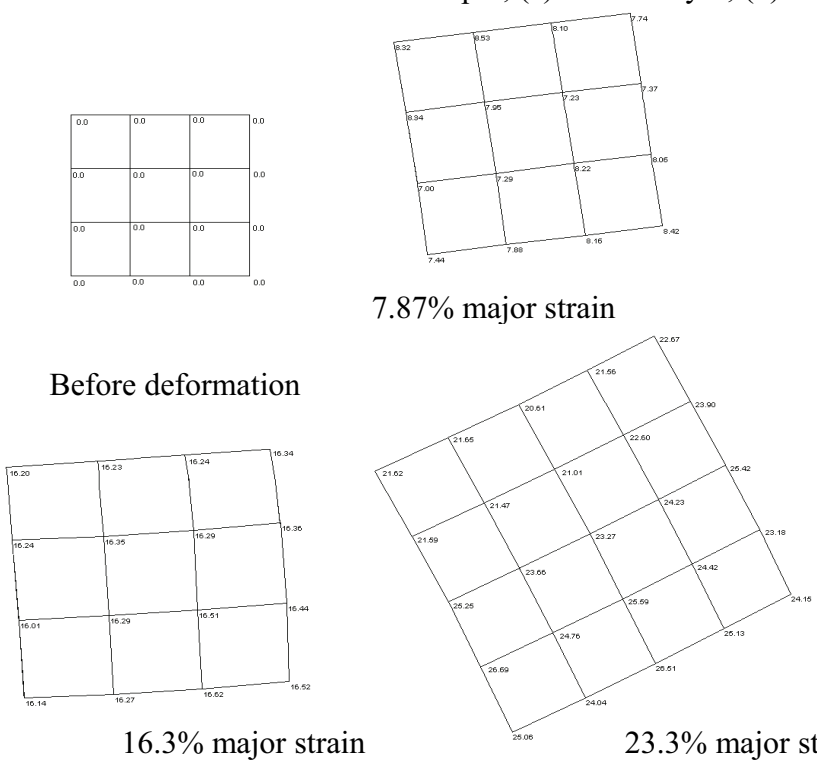


Fig. 2 Result from strain analysis of the four samples after and before biaxial deformation

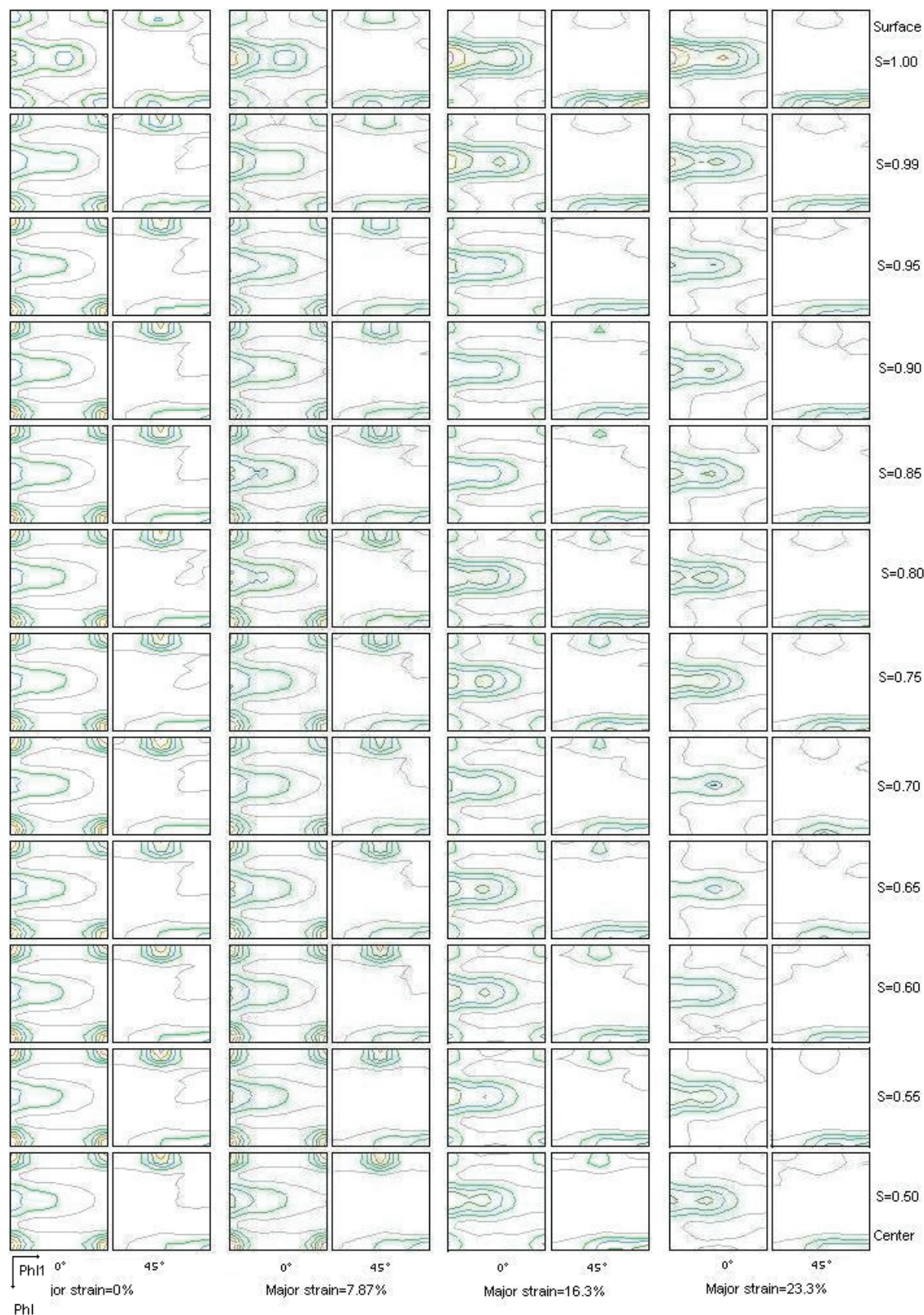


Fig. 3 Orientation distribution functions ($\varphi_2=0^\circ, 45^\circ$) at different deformation degrees

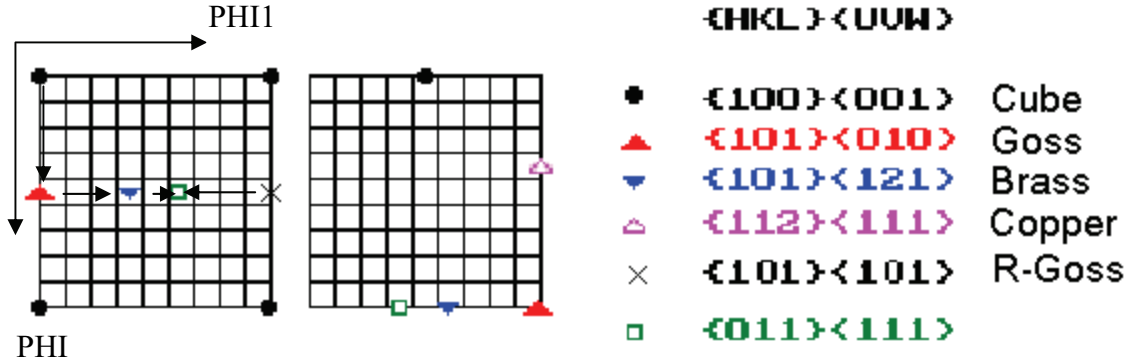


Fig. 4 Positions of six ideal orientations in Euler space

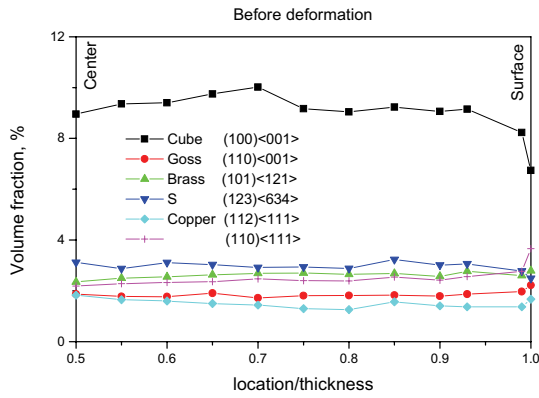


Fig. 5 Volume fraction before deformation

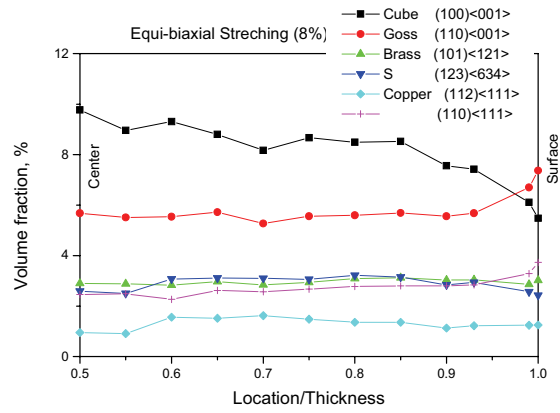


Fig. 6 Volume fraction at 7.87% major strain

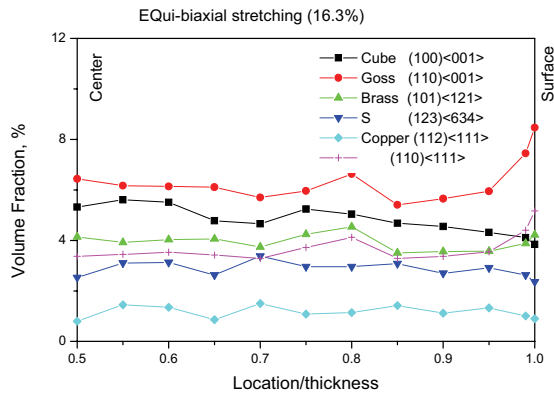


Fig. 7 Volume fraction at 16.3% major strain

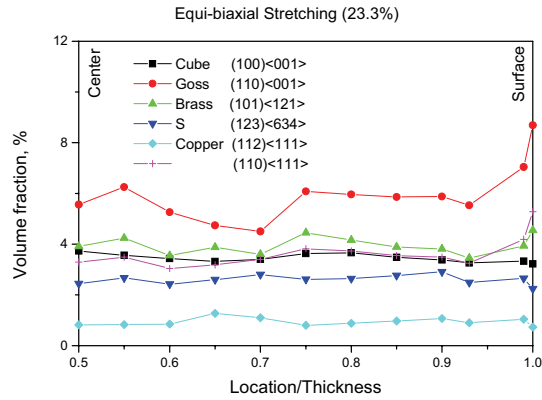


Fig. 8 Volume fraction at 23.3% major strain